

# ANALYTICAL MODEL FOR PREDICTING THE CHARACTERISTIC PROPERTIES OF SHAPE MEMORY ALLOYS

CHRISTIAN BRECHER<sup>1</sup>, NICLAS KLUMPEN<sup>1</sup>, STEPHAN NEUS<sup>1</sup>,  
MATTHIAS MARX<sup>1</sup>

<sup>1</sup>RWTH Aachen University, Laboratory for Machine Tools and  
Production Engineering, Aachen, Germany

DOI: 10.17973/MMSJ.2025\_03\_2024122

N.Klumpen@wzl.rwth-aachen.de

Passive vibration isolation is a key factor in achieving precise results in milling processes and extending the service life of tools. An innovative approach involves using damping elements made from NiTi shape memory alloys. This approach is based on the alloys ability to convert large amounts of mechanical energy into thermal energy through the pseudo-elastic effect, with the pronounced transformation hysteresis of the material providing its damping potential. While previous experimental studies have offered valuable insights, analytical models are essential for accurately predicting the complex behavior of these materials. Therefore, the present work aims to develop an analytical model capable of predicting the characteristic properties of shape memory alloys under dynamic compressive loading. This not only offers a deeper understanding of the underlying physical mechanisms but also provides a solid foundation for the optimization and application of these alloys in real-world scenarios.

## KEYWORDS

Shape memory alloys, characteristic properties, damping, hysteresis characteristics

## 1 INTRODUCTION

Since the discovery of the shape memory effect in the 1930s, research in this field has steadily increased, focusing on characterizing material behavior and developing models to describe it. SCHÄFER conducted a comprehensive literature review to identify suitable models for simulating the nonlinear, superelastic properties of shape memory alloys, evaluating over 130 publications. Through a step-by-step reduction of the models based on criteria such as superelasticity and stress-induced phase transformation, a utility analysis was finally conducted, identifying the SCHMIDT model as the most suitable. [SCHÄFER 2022] The SCHMIDT model is a one-dimensional model based on the theory of plasticity, assuming a quasi-static hysteresis while considering temperature-related influences. Its application is limited to calculating the stress curve for a given strain. [SCHMIDT 2004] However, since the SCHMIDT model is idealized and does not account for dynamic effects, an extension of the approach is necessary. This extension aims to enable the modeling of the essential properties of shape memory alloys (SMA) under various dynamic compressive loads and to determine their damping potential. Several recent studies have attempted to refine and expand analytical models for SMA behavior. LAGODAS provide a comprehensive overview of the modeling of shape memory alloys. The work covers thermomechanically coupled models for stress- and temperature-induced phase transformation, incorporating

hysteresis effects, microstructural influences, and multiscale approaches for more accurate SMA simulations. However, the focus is primarily on quasi-static loading, while dynamic effects and viscoplastic phenomena are insufficiently addressed. In particular, a detailed analysis of high-frequency damping behavior is lacking, limiting the applicability to dynamic load cases and highlighting the need for further research. [LAGODAS 2012] HEIN introduced a thermodynamically consistent model that incorporates velocity-dependent effects in superelastic SMA behavior. While this approach enhances the accuracy of rate-dependent responses, it remains constrained to quasi-static conditions and does not fully capture dynamic effects. [HEIN 2018] CISSÉ conducted a comprehensive review of constitutive models for SMAs, analyzing different approaches to capturing phase transformations and mechanical responses. Their work highlighted the necessity of developing models that integrate both thermal and mechanical loading conditions while improving computational efficiency. However, most reviewed models still lack detailed descriptions of damping behavior under dynamic compressive loading. [CISSÉ 2016] Additionally, VEDAMANICKAM developed a theoretical framework to design Ti-based SMAs by correlating composition with electronic properties and transformation temperatures. Their study focuses on material design for high-temperature applications, yet does not address the need for an analytical model that predicts SMA damping behavior under various dynamic loading conditions. [VEDAMANICKAM 2023]

While these studies provide valuable insights into SMA modeling, they primarily focus on quasi-static conditions and neglect essential aspects of high-frequency damping behavior under dynamic compressive loads. The existing models, including the SCHMIDT model, offer a strong foundation but require further refinement to incorporate viscoplastic effects and transient loading responses. This study aims to bridge this gap by proposing an enhanced analytical model that not only improves predictive accuracy but also extends the applicability of SMAs in damping applications under dynamic conditions.

## 2 ANALYSIS OF THE BASIC MODEL

The SCHMIDT model focuses on calculating the stress curve of superelastic NiTi-SMAs at a given strain, assuming that damping is caused by the movement of lattice defects occurring during deformation. These lattice defects arise from mechanisms such as dislocation movements, phase transitions, or diffusion processes. The model also considers microstructural properties of the alloy, including the size of the martensite and austenite phases as well as the distribution of lattice defects. It is based on a rheological Prandtl model, which consists of a Hook element and a St. Venant element that describe the elastic and plastic contributions to the phase transformation. The model's yield criteria enable the prediction of the damping capacity of NiTi-FGL under various boundary conditions by mapping both the forward and reverse transformations between martensite and austenite. [SCHMIDT 2004]

### 2.1 Description of the basic model

The significant slope of the plateau during transformation is described by a hardening law based on constitutive equations. In the quasi-static isothermal case, a distinction can be made between the ideal-plastic and isotropic hardening laws. According to the extended Prandtl model, the total strain  $\varepsilon$  consists of an elastic component  $\varepsilon^{el}$  and a plastic component  $\varepsilon^{Tr}$ , referred to as the transformation strain:

$$\varepsilon = \varepsilon^{el} + \varepsilon^{Tr} \quad (1)$$

The elastic component  $\varepsilon^{el}$  represents the reversible strain that decreases when the material is unloaded, while the plastic

component  $\varepsilon^{Tr}$  describes the irreversible strain that occurs during the superelastic transition due to the transformation of the crystal structure. For the stress in the linear elastic region, based on Hooke's law, the following applies:

$$\sigma = E \cdot \varepsilon^{el} = E(\varepsilon - \varepsilon^{Tr}) \quad (2)$$

The slope of the plateau in the transformation region is limited by the internal variable  $\alpha$  and the maximum transformation strain  $\varepsilon_{gr}^{Tr}$ . The internal variable  $\alpha$  reflects the transformation strain and is limited by the complete transformation:

$$\alpha = \varepsilon^{Tr} \quad (3)$$

In the transformation region, negative strain rates are possible, allowing the hysteresis to be divided into forward and reverse transformations. A fixed parameter  $K$  is assumed for isotropic hardening. The transformation condition for the forward transformation is described in equation (4) and the transformation condition for the reverse transformation is described in equation (5):

$$f^h(\sigma, \alpha) = \sigma - [\sigma_{Fh} + K \cdot \alpha] \text{ for } \dot{\varepsilon} > 0 \quad (4)$$

$$f^r(\sigma, \alpha) = \sigma - [\sigma_{Fr} + K \cdot \alpha] \text{ for } \dot{\varepsilon} < 0 \quad (5)$$

The differing elastic moduli of austenite and martensite are accounted for by a linear dependence on the transformation strain. A Voigt model, representing a series connection of austenitic and martensitic springs, is used, as shown in Equation (6):

$$E = E_A - \frac{\varepsilon^{Tr}}{\varepsilon_{gr}^{Tr}} (E_A - E_M) \quad (6)$$

The transformation conditions are extended by a temperature-dependent back stress  $q$  to adjust the transformation stress to a given temperature. The Clausius-Clapeyron principle is used to calculate the back stress:

$$f^h(\sigma, q, \alpha) = \sigma - [\sigma_{Fh} + q + K \cdot \alpha] \quad (7)$$

$$f^r(\sigma, q, \alpha) = \sigma - [\sigma_{Fr} + q + K \cdot \alpha] \quad (8)$$

$$q = H(T - T_0) \quad (9)$$

The temperature change is described by latent heat and heat exchange, using a Newton approach with a constant heat transfer coefficient  $\delta$ . The change is proportional to the transformation strain rate  $\dot{\varepsilon}^{Tr}$  and determined by the proportionality factor  $C$ .

$$\dot{T} = -\delta(T - T_R) + C \cdot \dot{\varepsilon}^{Tr} \quad (10)$$

## 2.2 Algorithmic implementation of the basic model

The algorithmic implementation of the SCHMIDT model involves solving the constitutive equations using a time-incremental predictor-corrector method, known as the return-mapping approach. In each time step, the heat exchange between the sample and the environment is calculated, starting with an update of the strain:

$$t_n = t_{n-1} + \Delta t_n \quad (11)$$

$$\varepsilon_n = \varepsilon_{n-1} + \Delta \varepsilon_n \quad (12)$$

Using the previous time step, an unchanged value for the transformation strain is assumed, and the current elastic modulus, test stress, and temperature-related back stress are determined:

$$E_n = E_A - \frac{\varepsilon_{n-1}^{Tr}}{\varepsilon_{gr}^{Tr}} (E_A - E_M) \quad (13)$$

$$\sigma_n^t = E_n(\varepsilon_n - \varepsilon_{n-1}^{Tr}) \quad (14)$$

$$q_n = H(T_{n-1} - T_0) \quad (15)$$

The test transformation functions  $f_n^{th}$  and  $f_n^{tr}$  are then calculated:

$$f_n^{th} = \sigma_n^t - [\sigma_{Fh} + q_n + K \cdot \varepsilon_{n-1}^{Tr}] \text{ for } \dot{\varepsilon} > 0 \quad (14)$$

$$f_n^{tr} = \sigma_n^t - [\sigma_{Fr} + q_n + K \cdot \varepsilon_{n-1}^{Tr}] \text{ for } \dot{\varepsilon} < 0 \quad (15)$$

Subtracting the test transformation function from the real transformation condition yields:

$$f_n^h - f_n^{th} = -E_n \Delta \varepsilon_n^{Tr} - H(T_n - T_{n-1}) - K \cdot \Delta \varepsilon_n^{Tr} \quad (16)$$

Assuming small time steps, the temperature change due to transformation strain can be simplified:

$$T_n - T_{n-1} = C(\varepsilon_n^{Tr} - \varepsilon_{n-1}^{Tr}) = C \cdot \Delta \varepsilon_n^{Tr} \quad (17)$$

This leads to the following equations for the transformation strain increment during forward and reverse transformations:

$$\Delta \varepsilon_n^{Tr} = \frac{f_n^{th}}{E_n + K + HC} \quad (18)$$

Finally, the real stress is calculated and the temperature is updated using:

$$T_n = (T_{n-1} + T_n^{Tr} - T_R) \cdot e^{-\delta \Delta t_{n-1}} + T_R \quad (19)$$

## 3 MODEL DESCRIPTION

The model by SCHMIDT, as described in Chapter 2, allows for the modeling of the static material behavior and the resulting stress-strain curve of an ideal SMA element. However, it has limitations with respect to dynamic material behavior, as it does not account for the viscoelastic properties that are relevant in practical applications. Furthermore, SMAs in practice often deviate from the ideal model (see Figure 1 for comparison).

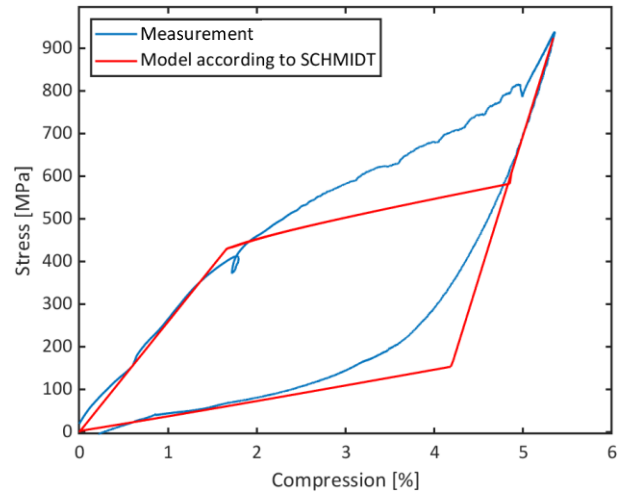


Figure 1 : Comparison of a measured stress-pressure hysteresis with that modeled according to SCHMIDT

The existing model is extended to better estimate the dynamic material behavior and the resulting damping effect. The extensions include:

1. Separate isotropic hardening
2. Parameter variation
3. Prediction of dynamic behavior through phase shift
4. Adjustment of temperature prediction
  - a. Iterative approach to account for dynamic effects
  - b. Separate temperature change for forward and reverse transformation
5. Calculation of damping coefficients

The following sections detail the specific adjustments made to the existing model for calculating the material behavior according to Schmidt. Unless otherwise specified, the equations from the original model are retained.

### 3.1 Addition of separate isotropic solidification

Metals behave linearly elastic under uniaxial loading until they reach the yield stress. Beyond the yield stress, the stress remains constant in the ideal plastic case. However, in materials with work hardening, the stress increases with increasing strain due to the hindrance of dislocation movement by lattice defects during plastic deformation, which requires higher stress for further deformation [MEYERS 1999].

SMA's also exhibit work hardening, meaning that the mechanical stress during phase transformation does not remain constant but increases with progressive plastic deformation. In the Schmidt model, this is accounted for by a linear isotropic hardening approach for both forward and reverse transformations, where the stress increases proportionally with the amount of transformed structure. The hardening parameter  $K$  determines the slope of the transformation plateau.

However, empirical stress-strain curves show that the slopes of the stress plateaus for forward and reverse transformations differ. Therefore, modeling with identical slopes, as in the original Schmidt model, would inadequately represent the real material behavior (see Figure 2).

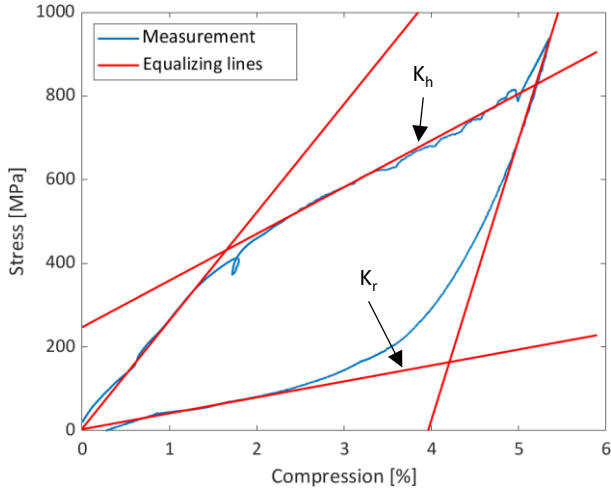


**Figure 2 :** Representation of the different isotropic hardening with a measured stress-pressure hysteresis

To improve the model's accuracy, the hardening parameters for the forward and reverse transformations are treated separately, with  $K_h$  for the forward transformation and  $K_r$  for the reverse transformation. The transformation test functions (Equations 14 and 15) and the calculation of the transformation strain increment (Equation 18) in a time step are adjusted accordingly:

$$f_n^{th} = \sigma_n^t - \sigma_{Fh} - q_n - K_h \cdot \varepsilon_{n-1}^{Tr} \quad (20)$$

$$f_n^{tr} = \sigma_n^t - \sigma_{Fr} - q_n - K_r \cdot \varepsilon_{n-1}^{Tr} \quad (21)$$

$$\Delta \varepsilon_n^{Tr} = \frac{f_n^{th}}{E_n + K_h + H \cdot C} \quad (22)$$

$$\Delta \varepsilon_n^{Tr} = \frac{f_n^{tr}}{E_n + K_r + H \cdot C} \quad (23)$$

These adjustments allow for a more accurate modeling of the material behavior of SMA's by accounting for the different hardening effects during phase transformations.

### 3.2 Scattering of parameters to map the inhomogeneity of the material

By separating the isotropic hardening for the two transformation regions, the material behavior of shape memory alloys can be described with a seven-parameter superelasticity model. While the ideal model assumes sharp transitions between the elastic regions and the phase transformations, real load curves often do not exhibit clear kinks at these transitions (areas A and B). Figure 3 illustrates that in practice there are often deviations between the measured hysteresis and the theoretical approximation curves of the model, particularly in the initial region of the reverse transformation (area B), which is difficult to avoid even with optimal model parameterization.

The deviations result from inhomogeneities in the material and the mechanical stress state. Varying grain sizes lead to uneven mechanical stresses, causing the phase transformation to occur non-uniformly throughout the material. Additionally, an

inhomogeneous temperature distribution arises under load, as the transformation initially occurs in specific regions, leading to local heating. This heating affects the yield stress of the surrounding areas, which increases proportionally to the temperature [LANGBEIN 2014, KAACK 2002].

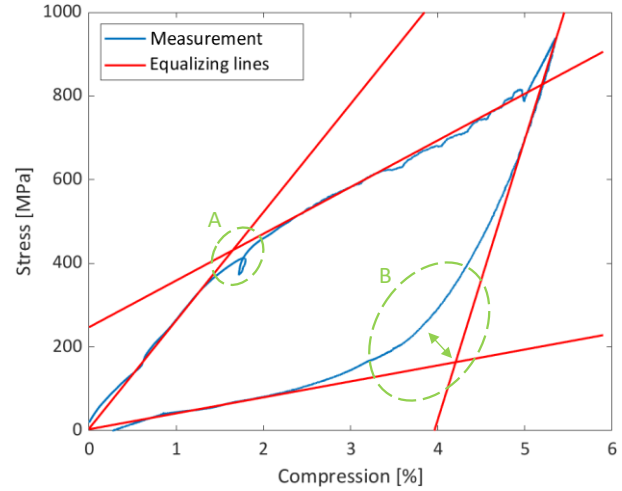


**Figure 3 :** Measured stress-compression hysteresis of a compression test with determined material parameters

The extended model accounts for these inhomogeneities by applying a standard distributed scatter  $s$  to the material parameters  $P$ . Consequently, the phase transformation is not represented abruptly, but gradually, resulting in a more realistic depiction of the stress-strain hysteresis.

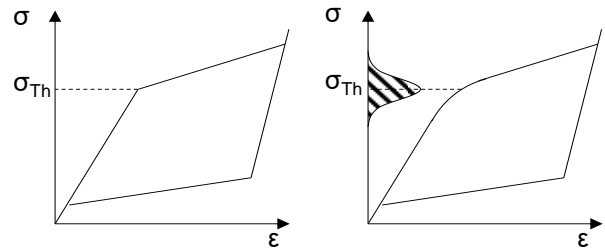


**Figure 4 :** Schematic representation of the stress-strain hysteresis with and without scattering of the parameter

The model algorithm calculates the material behavior by considering the scattering through the creation of multiple individual stress curves  $k$ , each based on samples of the scattered parameters. The input signal remains identical for all curves, and the stress curves are then arithmetically averaged at each time step to determine the resulting force curve.

$$P_k = P \pm s \quad (24)$$

$$\sigma(t) = \frac{1}{k} \sum_k \sigma_k(t) \quad (25)$$

To achieve a representative match with the standard distribution of the parameters, it is advisable to calculate a large sample size or many individual curves. The scatter of the parameters is determined manually to approximate the measured behavior as accurately as possible.

### 3.3 Prediction of dynamic behavior through phase shift

Viscoelasticity describes the property of a material to exhibit both elastic and viscous behavior under load. In elastic materials, stress and strain are in phase, whereas in viscous materials, strain lags behind stress, with a possible phase shift of up to  $90^\circ$ . In viscoelastic materials, the phase shift ranges between  $0^\circ$  and  $90^\circ$ , depending on damping, frequency, amplitude, and temperature. In metallic materials, the phase shift is primarily caused by lattice defects [MEYERS 1999].

In the case of forced harmonic oscillations outside the resonance frequency, the load curve of metals exhibits an elliptical expansion due to the phase shift. SCHMIDT defines the phase shift via the lag angle of the strain  $\epsilon$  after the stress  $\sigma$ , but this was not implemented in the calculation model. Dynamic effects are considered only through time-dependent thermal relationships.

Based on the empirical measurement data from a compression test shown in Figure 5, it can be confirmed that a phase shift occurs under forced harmonic loading.

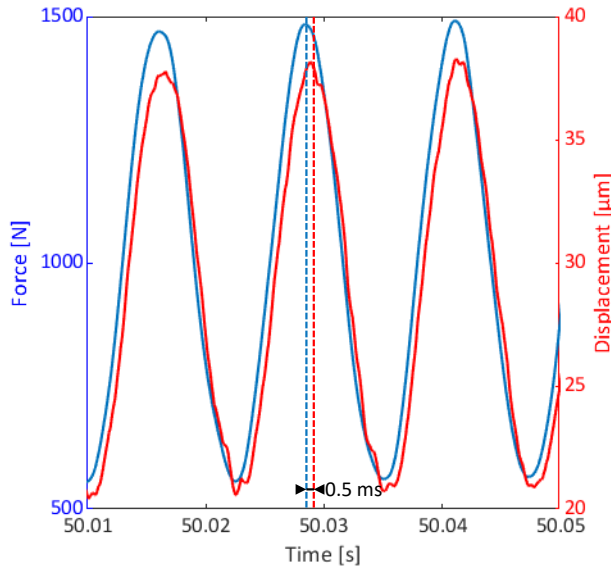


Figure 5 : Phase shift between the strain  $\epsilon$  and stress  $\sigma$

The signal section shows a constant phase shift of around 0.5 ms between the force and displacement signals under cyclic load. Vibration tests with varying frequencies indicate that the phase shift remains constant but increases relative to the period duration as the frequency increases. Consequently, the hysteresis becomes wider at higher frequencies, leading to a higher damping effect of the material.

To account for the dynamic effect, the phase shift is implemented in the model by introducing a time shift  $\varphi$ . After calculating the static force curve, the stress curve is shifted by  $p$  increments, based on the ratio of the phase shift to the duration of a time increment. The value is rounded, as only integer time increments are used. The corrected dynamic stress curve is therefore identical to the static curve, but shifted by  $p$  time increments:

$$p = \text{round}\left(\frac{\varphi}{\Delta t}\right) \quad (26)$$

$$\sigma_{dyn}(n) = \sigma(n + p) \quad (27)$$

Due to the phase-shifted stress, the load curve widens elliptically. In the normally linear load ranges, energy dissipation occurs due to the frequency-dependent hysteresis.

### 3.4 Adjustment of temperature prediction

There are two basic approaches in the literature for modeling and calculating the temperature change due to phase transformation:

#### Approach 1 - Latent Heat:

This approach states that the heating caused by the phase transformation is proportional to the transformation strain. The temperature increases uniformly with the amount of transformed structure, with the heating during the forward transformation corresponding to the cooling during the reverse transformation. Therefore, the temperature remains constant under cyclic loading. The SCHMIDT model accounts for this

approach through the proportionality factor  $C$ , which represents the relationship between transformation strain and temperature change.

#### Approach 2 - Dissipated Energy:

This approach calculates the dissipated energy based on the law of conservation of energy, where mechanical energy is converted into elastic (spring) and dissipated energy. The dissipated energy is graphically determined by the hysteresis area minus the elastic energy. The SCHMIDT model does not consider this approach. To extend the model, the dissipated energy is calculated for each time step  $n$  using the following formula.

$$E_{diss}(n) = V \cdot \sigma_{dyn}(n) \cdot (\epsilon_{tr,dyn}(n) - \epsilon_{tr,dyn}(n-1)) \quad (28)$$

The newly created hysteresis area is used here as the product of transformation strain, mechanical stress, and sample volume. With a sufficiently small step size, it can be assumed that  $\sigma_{dyn}(n) \approx \sigma_{dyn}(n-1)$ . The temperature change due to the dissipated energy is determined by Equation (29).

$$C_W = \frac{E_{diss,n}}{\Delta T} \leftrightarrow \Delta T = \frac{E_{diss,n}}{C_W} \quad (29)$$

This approach states that the heat generated during the forward transformation is greater than the cooling during the reverse transformation, leading to heating of the material under cyclic loading. This approach also considers the damping effect due to the phase shift under harmonic loading.

To incorporate both approaches, SCHMIDT's model is extended to include the temperature change due to dissipated energy. The temperature change is calculated as the quotient of the dissipated energy and the heat capacity of the material  $C_W$ .

$$T_n = \left( T_{n-1} + E_{lat} + \frac{E_{diss,n}}{C_W} - T_R \right) \cdot e^{-\delta \cdot \Delta t_{n-1}} + T_R \quad (30)$$

$$E_{lat} = C \cdot (\epsilon_n^{Tr} - \epsilon_{n-1}^{Tr}) \quad (31)$$

In Schmidt's model, the temperature change is calculated in parallel with the static behavior, which does not account for the dissipated energy and its additional heat due to hysteresis, potentially leading to inaccuracies. As a solution, an iterative method is implemented to consider these effects (see Figure 6).

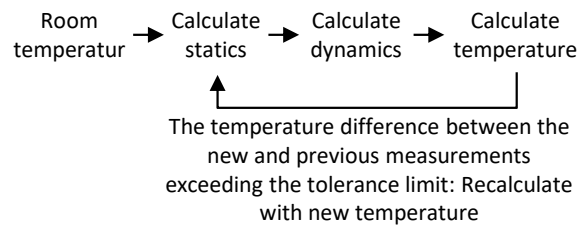


Figure 6 : Iterative method for determining the sample temperature

In the first run, the calculation is performed with a constant room temperature. The dissipated energy, latent heat, and temperature curve are then calculated and used in the next iteration. The temperature curve converges quickly, as the mechanical behavior changes only slightly.

Figure 7 shows the temperature curves of various iterations. The temperature curve converges quickly, although differences can still be observed between the 2nd (blue) and 3rd (red) iterations, while the 3rd and 4th (yellow) iterations are almost identical.

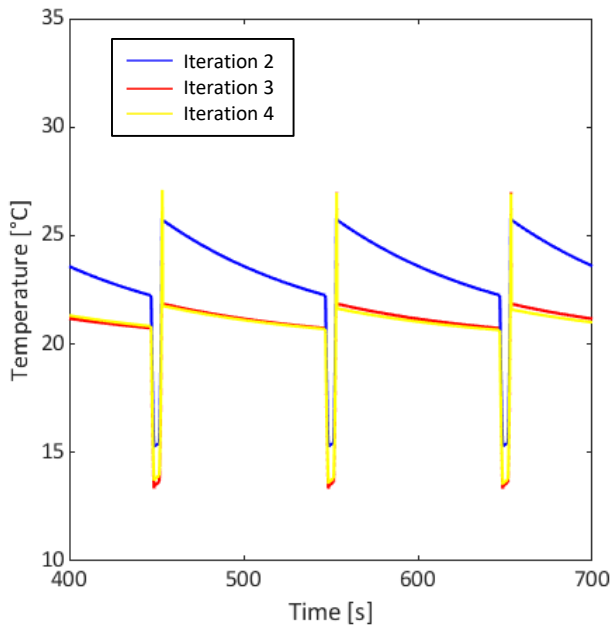


Figure 7 : Section of temperature curves of various iterations

### 3.5 Calculation of damping coefficients

To determine the damping effect of the material under the specified mechanical and thermal load, it is advisable to calculate the standardized damping characteristics. The basis for the calculation is the dynamic force curve and the underlying excitation signal. The damping parameters are determined as follows:

- Damping ratio  $D = \frac{1}{2 \cdot Q}$
- Attenuation factor  $d = \frac{1}{Q}$
- Quality factor  $Q = 2 \cdot \pi \cdot \frac{E_{max}}{E_{diss,cycle}}$

The dissipated energy per load cycle can be determined from the calculated course of the dissipated energy using defined limits:

$$E_{total,cycle} = E_{diss,ges}(n_{end}) - E_{diss,total}(n_{start}) \quad (32)$$

$$E_{diss,total}(n) = \sum_{j=1}^n E_{diss,cycle}(j) \quad (33)$$

The maximum dynamic vibration energy is calculated according to the maximum spring energy, which is proportional to the dynamic stress and strain [SCHMIDT 2004].

## 4 ALGORITHMIC IMPLEMENTATION OF THE EXTENDED BASIC MODEL

The algorithmic implementation of the extended basic model aims to predict the mechanical stress based on a given uniaxial strain signal and to evaluate the material behavior with regard to damping. The calculation algorithm consists of an upstream and a downstream structure.

In the first step, the parameters for the superelasticity model are determined by evaluating stress and strain data from a compression test. Manually defined support points enable the calculation of fitting lines for the elastic regions and the transformation regions. The seven superelasticity parameters are derived from these line equations and their intersection points.

In the next step, the parameters are scattered to represent the inhomogeneous material behavior. A large sample of random parameter sets is generated and used to calculate the individual

stress curves. The calculated parameters are then used to determine a single stress curve.

- **Scattered parameters:** A sample of the scattered parameters for the superelasticity model.
- **Excitation parameters:** Define the strain input signal with a harmonic sine wave, frequency, and strain amplitude, as well as the number of discrete points per cycle to optimize model accuracy.
- **Constant parameters:** Material or environmental parameters that are assumed to be constant and are not scattered; they remain the same for all stress histories.

Modulus of of austenite	$E_A$	N/mm <sup>2</sup>
Modulus of elasticity of the martensite/stiffness after the plateau	$E_M$	N/mm <sup>2</sup>
Conversion voltage for load (back transformation A → M)	$\sigma_{Fh}$	N/mm <sup>2</sup>
Conversion voltage for relief (reverse transformation M → A)	$\sigma_{Fr}$	N/mm <sup>2</sup>
Maximum transformation strain	$\varepsilon_{gr}^{Tr}$	-
Parameters for isotropic hardening (plasticity modulus)	$K$	-
Temperature for which the transformation stresses were determined	$T_0$	°C
Room temperature	$T_R$	°C
Tension rise due to temperature increase (Clausius-Clapeyron factor)	$H$	-
Temperature decay coefficient	$\delta$	-
Coefficient for temperatuelasticityre rise due to conversion heat	$C$	-

Table 1. Model parameters for the calculation algorithm

Table 1 visualizes the model parameters for the calculation algorithm.

In the next step, the algorithm calculates the various individual stress curves within the downstream structure based on the specified parameters. This structure uses Schmidt's equations and the presented adjustments to determine the course of the mechanical stress from the discrete-time strain signal over a specified number of time steps.

In the first loop of the downstream structure, the transformation strain and the mechanical stress are calculated for each discrete point using Schmidt's modified approach. Initially, the stress is determined as a test under the assumption of elastic behavior. Then, the yield conditions for the phase transformations are checked, and a distinction is made between elastic behavior, forward transformation, or reverse transformation. Accordingly, the transformation strain and stress are calculated for each step using data from the current and previous time steps. This process is continued until the end of the signal.

After the signal ends, the mechanical stress signal is phase-shifted according to the approach for viscoelastic material behavior under harmonic oscillation. Based on the corrected stress curve, the temperature curve is calculated, which accounts for latent heat and dissipated energy. This temperature curve is used in the next iteration of the stress calculation, as the mechanical behavior is temperature-dependent. The steps are repeated until the difference between the temperature curves of the current and previous iterations is below the specified tolerance value.

The described method for calculating the mechanical stress is applied for each scattered parameter set, resulting in a defined number of different stress curves based on the same input signal. These individual curves are then arithmetically averaged for each time step to determine the final stress curve. Based on this stress curve and the input signal, the required energy curves and damping parameters, such as damping ratio, damping factor, and quality factor, are determined.

## 5 APPLICATION OF THE EXTENDED BASIC MODEL

To evaluate the suitability of the presented model for predicting the mechanical stress state and the dissipated energy in the context of the hysteresis surface, an empirical parameterization based on measured data is essential. This parameterization aims to adjust the idealized model to account for dynamic effects and to achieve optimal agreement with the experimental data. The overarching goal is to enable the model to accurately represent real load conditions.

To adapt the calculation algorithm and the extended model to a specified alloy composition and the corresponding heat treatment parameters, the required model parameters must be determined both empirically and based on literature values and material data sheets. This process follows the algorithmic implementation described in Chapter 4. Experimentally generated data is used to empirically determine the material-specific parameters.

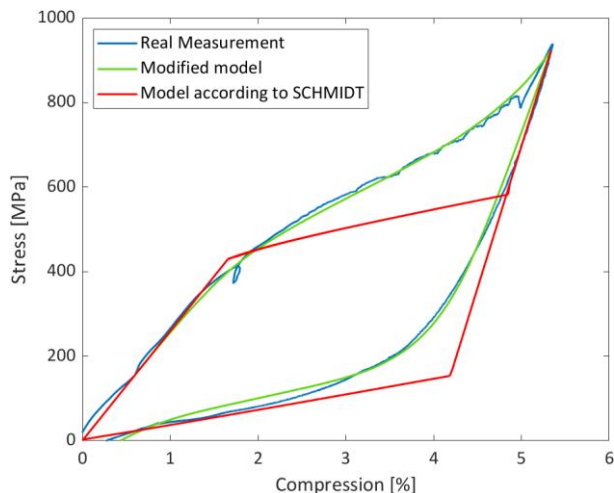


Figure 8 : Section of temperature curves of various iterations

Figure 8 presents a comparison of a real measured curve, the modeled curve according to SCHMIDT, and the curve of the modified model. This illustration shows that the modeled curve of the modified model is almost identical to the real measured curve. This highlights the ability of the extended model to accurately predict real mechanical loading conditions and the associated dissipative effects.

## 6 CONCLUSIONS

By extending the existing SCHMIDT model and incorporating the measures described in Chapters 3 and 4, a comprehensive and detailed model of superelastic behavior is developed. This extended model is able to accurately capture and simulate both the intrinsic material properties and external influences on the material behavior. As a result, the essential properties of shape memory alloys can be realistically represented under various load conditions. However, it is crucial to note that changes in alloy composition or adjustments to heat treatment parameters require careful readjustment of the model parameters in the modified model to maintain the accuracy and reliability of the simulations.

## ACKNOWLEDGMENTS

The authors would like to thank the Federal Ministry of Economics and Climate Protection (BMWK) for supporting this research under the project: Development of a SMA-based sensor system for monitoring tool clamping in PTI interfaces (SensoWEin). The project number is KK5046713KP3.

## REFERENCES

- [CISSE 2016] C. Cisse, W. Zaki, Zineb T. Ben. A review of constitutive models and modeling techniques for shape memory alloys. *Int J Plast*, 76, 2016
- [HEIN 2018] Hein, A.: Auslegung und Entwurf adaptiver Strukturen und Systeme mit Formgedächtnislegierungen. Bericht Nr. 705. Institut für Konstruktionstechnik und Technisches Design, Universität Stuttgart, 2018
- [KAACK 2002] Kaack, M.: Elastische Eigenschaften von NiTi-Formgedächtnis-Legierungen. Bochum, Doctoral thesis, 2002
- [LAGOUDAS 2012] Lagoudas, D. C. (Hrsg.): Shape Memory Alloys: Modeling and Engineering Applications. 1st ed. Springer, New York, 2012
- [LANGBEIN 2014] Langbein, S.: Konstruktionspraxis Formgedächtnistechnik. Potentiale - Auslegung - Beispiele. 1st ed. Aufl. Wiesbaden: Springer Fachmedien Wiesbaden GmbH, 2013
- [MEYERS 1999] Meyers, M. A.; Chawla, K. K.: Mechanical behavior of materials. Aufl. Upper Saddle River, NJ: Prentice Hall, 1999
- [SCHÄFER 2022] Schäfer, A.: Werkzeugseitiger Einsatz von NiTi-FGL zur Verbesserung der dynamischen Prozessstabilität bei der Fräsbearbeitung. Doctoral thesis, 2022
- [SCHMIDT 2004] Schmidt, I.: Untersuchungen zur Dämpfungskapazität superelastischer Nickel-Titan-Formgedächtnislegierungen, 2004
- [VEDAMANICKAM 2023] Vedamanickam, S.; Vageeswaran, P.; Jacob, B.: Theoretische Analyse und Design von Formgedächtnislegierungen auf Ti-Basis mit Korrelation zwischen Zusammensetzung und elektronischen Eigenschaften und Umwandlungstemperaturen für Hochtemperaturanwendungen. *Materialwissenschaft und Werkstofftechnik: B*, Bd. 296, 2023

**CONTACTS:**

M.Sc. Niclas Klumpen  
RWTH Aachen University  
Laboratory for Machine Tools and Production Engineering  
Steinbachstraße 19, Aachen, 52074, Germany  
+492418027441  
N.Klumpen@wzl.rwth-aachen.de